GEOPHYSICAL RESEARCH LETTERS, VOL. 32, L21101, doi:10.1029/2005GL023656, 2005

Periodic intensity variations in global ENA images of Saturn

C. Paranicas, D. G. Mitchell, E. C. Roelof, P. C. Brandt, D. J. Williams, S. M. Krimigis, and B. H. Mauk

Applied Physics Laboratory, Johns Hopkins University, Laurel, Maryland, USA

Received 27 May 2005; revised 27 September 2005; accepted 22 August 2005; published 2 November 2005.

[1] During select time periods in orbit about Saturn, Cassini's Ion and Neutral Camera (INCA) has detected a periodic global ENA signal. Images taken during such periods reveal the presence of a rotating source component in addition to a steady-state component; both components have peak brightness in the midnight sector, when viewed from near dawn. We present a model that synthesizes some of the basic features of the data and gives good agreement with the integrated signal. Both components, as well as the Compton-Getting effect whose importance was previously unrecognized in ENA imaging, are needed to explain some aspects of the data. **Citation:** Paranicas, C., D. G. Mitchell, E. C. Roelof, P. C. Brandt, D. J. Williams, S. M. Krimigis, and B. H. Mauk (2005), Periodic intensity variations in global ENA images of Saturn, *Geophys. Res. Lett.*, *32*, L21101, doi:10.1029/2005GL023656.

1. Introduction

[2] The Ion and Neutral Camera (INCA) on Cassini is one of three sensors that make up the Magnetosphere Imaging Instrument (MIMI). INCA images energetic neutral atoms (ENAs) that emanate primarily from Saturn's inner magnetosphere. As energetic ions are transported radially inward, they encounter an ambient population of neutral gas associated with Saturn's icy moons and E-ring [*Richardson*, 1998; *Shemansky et al.*, 2004]. The observed ENAs are likely created at the periphery of the neutral cloud, where charge exchange collisions are highly probable and yet ENAs can freely exit the system without subsequent stripping collisions.

[3] Because ENAs can travel great distances in gas-less space, INCA was able to detect Cassini's magnetosphere from a distance of 500 Saturn radii (R_S) during its approach to Saturn. INCA is bore-sighted to within 9.5° of the optical instruments, and the pointing was usually favorable for imaging the entire magnetosphere. At these times, the entire magnetosphere was imaged in a few detector pixels at very low counting rates, so the spatial structure of the emission region could not be resolved. During approach, the few-pixel signal varied by up to an order of magnitude, suggesting transient processes. We often observed periods when the magnetospheric signal was below our detector threshold; in one instance we observed a rotation-modulated signal for almost two days, but in general the observation periods were too short, and the signal too weak to detect modulations.

[4] At the other extreme, during Saturn Orbit Insertion (SOI) in July, 2004, the ENA image consisted of many illuminated pixels, so INCA could resolve a localized ENA emission whose source population of ions corotated from the day side to the night side in the few hours of observation [*Krimigis et al.*, 2005]. Krimigis and his colleagues noted that the emission increased in brightness as it moved toward the midnight sector. In this paper, we concentrate on a third period, at the end of 2004, when the spacecraft was near local dawn. Images from the December, 2004 period again show variations in the ENA signal. The images also tend to appear brightest on the anti-sunward side of the planet. We are frequently able to discern the presence of a rotating feature in sets of consecutive images. As reported by *Krimigis et al.* [2005], there appears to be an overall ~11 hour periodicity to the ENA signal from the entire magnetosphere. In this paper, we use a model consisting of a symmetric population of ions and a corotating population to qualitatively reproduce several features of the images. It is only when we take into account details of the spacecraft distance from the ENA production region, and other ion measurement effects, that we come close to quantitatively replicating the behavior of the image-integrated signal.

2. Observations

[5] ENAs are created when singly charged energetic ions undergo charge exchange with ambient neutrals. Since very little energy is lost in the charge-exchange process, an ENA has approximately the same energy as its parent ion. INCA is a time-of-flight instrument that images ENAs in discrete energy passbands from a few to a few hundred keV. The instrument field-of-view is 120° × 90° sampled in images of up to 64 × 64 pixels. Before encountering the front detector foil, particles must pass through a fan of high voltage deflection plates, which, when turned on, efficiently sweep out charged particles [*Mitchell et al.*, 1998]. Hydrogen and oxygen ENAs generate much different multiplicities of secondary electrons in triggering the back-plane microchannel plate, so discrimination between them is usually possible. For a particular energy, hydrogen ENAs typically scatter less in the front foil than oxygen, so hydrogen ENA images have considerably better resolution. A complete description of MIMI and its component sensors is given by *Krimigis et al.* [2004].

[6] In Figure 1, we present two INCA images from December 20, 2004 (day 2004–355). The images are smoothed with a boxcar algorithm that leaves the center of individual pixels unchanged and blends the hard edges between adjacent pixels. The images display intensities of 20–50 keV hydrogen ENAs at times approximately half a Saturn rotation apart. During this period, Cassini was south of Saturn's spin equator and traveling away from the planet, through a radial distance of about 40 R_S. A grid showing a

0094-8276/05/2005GL023656$05.00

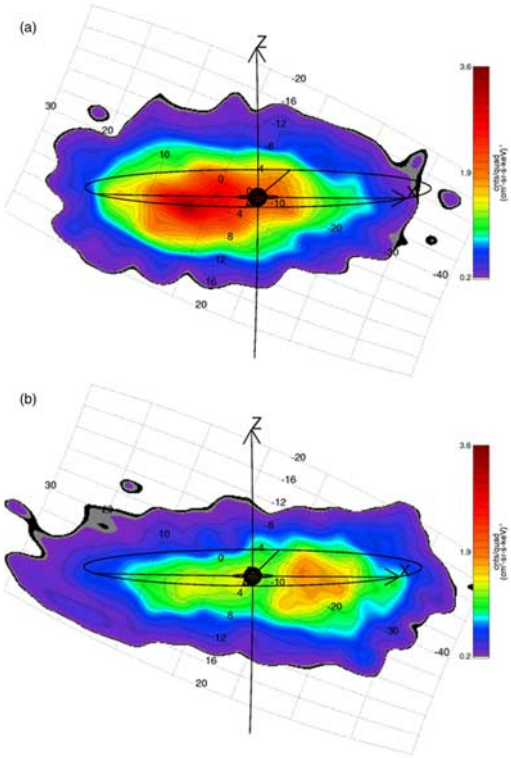

Figure 1. Smoothed INCA ENA images of Saturn's magnetosphere from below the planet's spin equator. Differential intensity in counts/(cm^2-s-sr-keV) of 20–50 keV H ENAs are presented for two 28 minute periods on December 20, 2004. Panel (a) shows 12:02 to 12:30 UT when the s/c was at about 39.8 R_S, 5° south latitude and a local time of 0535 and (b) shows 17:22 to 17:50 UT when the s/c was at about 40.8 R_S, 5° south latitude, and at a local time of 0539. The 120° × 90° INCA field-of-view is cropped to highlight the main features of the image with contours indicated. Saturn and the main rings are sketched in.

section of the INCA field-of-view is drawn as well as the location of Saturn, the main rings, and Titan's orbit. Axes are drawn in the Saturn Equatorial System (SZS) with the z-axis parallel to Saturn's spin axis, y-axis in the direction of the cross product between the z-axis and the Saturn-to-Sun line, and the x-axis completing the right-hand system. Since the spacecraft is below the equator, we are looking slightly up at the oval of Titan's orbit in the x-y plane; the y-axis is pointing into the page and slightly to the left. Figures 1a and 1b give a sense of the variation in the ENA emission from the inner magnetosphere. The bright, predominantly night-side emission apparent in Figure 1a is greatly diminished about 5 hours later in Figure 1b, when a fainter dayside emission dominates the field-of-view.

[7] In Figure 2, we show oxygen images from near the end of the same day and the beginning of 2004-356. These data represent differential intensities of 64–96 keV oxygen ENAs, averaged over about 28 minutes. Because ions of differing energies drift differentially in the magnetic field (by gradient and curvature drift), they do not maintain a fixed longitudinal phase relationship with time; therefore, representative oxygen images are not contemporaneous with those for hydrogen. The display coordinates are the same as in Figure 1. Figure 2a shows the brightening in the midnight sector discussed above. Figure 2b, which is taken about 4 hours later, shows that this brightness has diminished significantly, with the midnight sector slightly brighter than the dayside sector. Both the hydrogren and oxygen images are representative of the images at other energies for each species detected during this period.

3. Modeling Considerations

[8] To get a sense of the relevant periodicities in these images over many days, we next present image-integrated counts as a function of time. Each data point in Figure 3 represents the sum of all counts in an image. Figure 3a shows hydrogen ENAs in the energy range 30–50 keV and Figure 3b shows oxygen ENAs in the range 64–96 keV. These plots of summed counts illustrate a fairly regular periodicity. Saturn's rotation rate, as defined by SKR (Saturn's kilometric radio emission), is about 10 hours 45 minutes and the peaks in both channels occur at about that frequency. Individual (un-summed) images obtained for these time periods sometimes show what we infer to be a spatially-confined corotating population of ions [*Paranicas et al.*, 2005]. Occurrences of this type of feature are present in

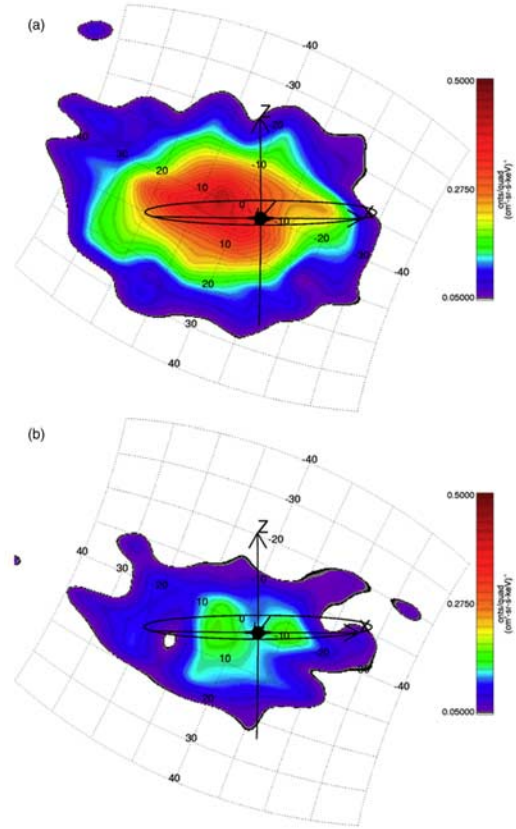

Figure 2. Same coordinate system as Figure 1. These two panels show the averaged differential intensity of 64–96 keV O ENAs. Panel (a) shows data from December 20, 2004 22:42–23:10 UT when Cassini was at 41.6 R_S, 5° south latitude, and near a local time of 0542, and panel (b) shows data from December 21, 2004 02:58–03:26 UT when the spacecraft was at 42.3 R_S, 5° south latitude and near a local time of 0544. See text for further details.

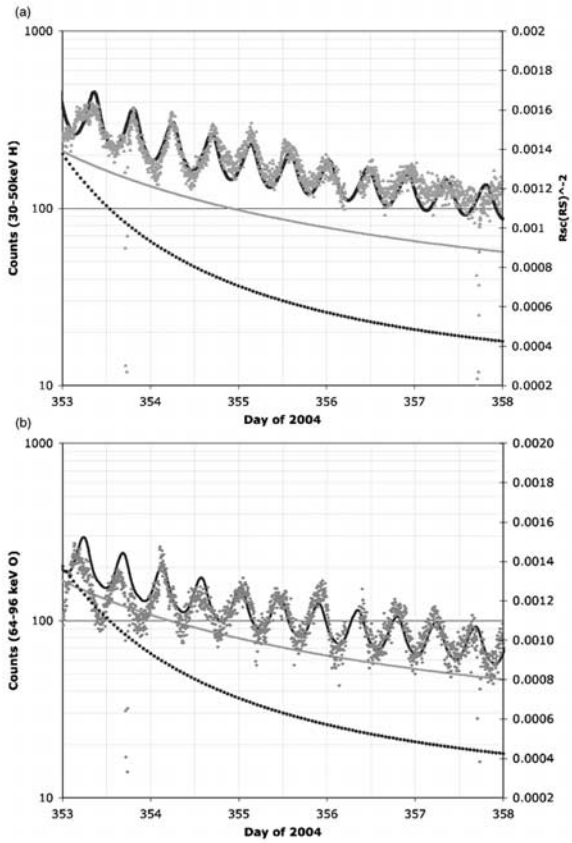

Figure 3. ENA counts summed over the entire image and plotted as a function of time. Panel (a) shows 30–50 keV H ENA data and panel (b) shows 64–96 keV O ENAs. Both panels include a solid gray line showing modeled total counts due to a symmetric ring distribution. The panels also show the modeled total counts due to both an axisymmetric ring distribution and a second distribution rigidly corotating with Saturn (solid black line). The s/c distance from Saturn, R^{-2}, is plotted as circles associated with the right-hand-side axis.

a small fraction of the data set suggesting to us that we are likely looking at transient processes, such as a series of repeated injections. In the hydrogen images, the corotating region can be the dominant signal in the image as in Figure 1b. The oxygen images also show corotating features but often these are dominated and/or obscured by the bright but steady emission coming from the midnight sector such as that in Figure 2a. Comparing the images and the summed counts, Figures 1a and 2a correspond to times when the summed counts are peaking whereas at the times of Figures 1b and 2b the summed counts are near local minima.

[9] An important feature of the data is the approximately R^{-2} falloff of the overall signal strength as the spacecraft moves away from the ENA source [see, for instance, *Mitchell et al.*, 2004]. During the time period in Figure 3a, Cassini moved from about 27 R_S near 04:40 LT at the beginning of 2004-353 to about 49 R_S and 06:07 LT at the beginning of day 2004-358. In Figures 3a and 3b, we show the R^{-2} of the spacecraft (where here R is the spacecraft distance from the planet in units of R_S), referenced to the right-hand-side axes. Both sets of data show that overall the detected counts are decreasing over this period. This would be approximately the expected falloff for a constant unresolved source of ENAs close to the planet. We discuss this further below.

[10] Another critical factor in understanding the basic aspects of these data is the Compton-Getting (CG) effect. The CG effect is a reference frame measurement effect that relates the particle count rates measured when the spacecraft frame and the rest frame of the plasma are moving relative to one another [*Gleeson and Axford*, 1968; *Roelof et al.*, 1976]. *Forman* [1970] gives a derivation of the CG anisotropy beginning with the Lorentz invariance of the phase space distribution function. *Ipavich* [1974] uses that formulation to derive a useful formula for how the measured count rates of energetic charged particles varies with angle to the flow,

$$C(\vartheta) = C(180)\left[\frac{1 - 2\alpha\cos\vartheta + \alpha^2}{[1+\alpha]^2}\right]^{-\gamma-1} \quad (1)$$

Here θ is the angle the plasma flow vector makes with the direction directly into the particle sensor, $\alpha = V_c/v$, where V_c is the relative speed between the convection frame and the spacecraft frame, v is the particle speed, γ (defined as - dlog j/dlog E, where j is the usual ion intensity) is the slope of the energy spectrum at energy E, and the count rate is normalized to the count rate when the detector is looking downstream (i.e. normalized to the minimum counting rate). The peak-to-valley ratio of the counts for 40 keV protons with $\gamma \sim 2.8$ in a plasma flowing at 90 km/s is approximately 1.7. For 80 keV O^+ with the same gamma and in the same plasma flow, the ratio is 4.3. By comparison, in Figure 3 the peak-to-valley ratio for H is $\sim$2 and for O it is $\sim$3.

[11] The Compton-Getting effect in the ions must be manifested in the ENAs that they create. When INCA images ENAs created from ions convected with a plasma flowing toward the sensor, it will measure higher counts of neutrals than when it detects ENAs created from ions convected with a plasma flowing away from the sensor, all other things being equal. When INCA is imaging the whole magnetosphere from dawn, the brightest emission region of a symmetric corotating population would therefore be on the midnight side of the magnetosphere. The CG effect could therefore explain the brightening discussed by *Krimigis et al.* [2005] during SOI when a corotating feature became brighter as it moved toward midnight (although an intensification of the ion feature itself cannot be ruled out in this observation that is over only a partial rotation).

[12] With these effects in mind, we sought to model the data assuming the ENA signal can be expressed as the sum of a steady axisymmetric component (a ring-like distribution) and a rotating component. We assume the axisymmetric component is centered at 10 R_S in both the hydrogen and oxygen models. We have plotted the emission from this component as a solid gray line in Figure 3. It is interesting to note that the intensities fall off slightly more slowly than the axisymmetric signal in both cases, and this is more apparent in the hydrogen.

[13] For completeness, we note that the axisymmetric distribution too has a CG modification when that component is resolved in an image. Such a distribution would be brighter near midnight if viewed from dawn (and this is how it is modeled here). However, in the image-integrated

intensities plotted in Figure 3, the CG effect due to an axisymmetric distribution will not produce a temporal variation in the signal; that variation must be due to a time-dependent component, e.g. an azimuthally asymmetric ion distribution that is rotating.

[14] We have assumed that the rotating component of the signal can be modeled as a point magnetospheric source rotating rigidly with the planet. It is assumed that ENAs are emitted steadily and isotropically from this point source. Such a model produces a variation in ENA-measured intensity as follows. As the magnetospheric plasma containing the point source rotates, the source moves alternately toward and away from the (retreating) spacecraft. The R^{-2} effect, enhanced by the CG effect, would then give a sinusoidal variation. Farther from the planet, the CG effect would dominate (where the fractional change in R during one rotation is negligible).

[15] In Figure 3a (Figure 3b), we take the point source to be at 8 R_S ($9R_S$). To fix the constant amplitude of the symmetric and rotating distributions, we used a least squares fit between the modeled signal (solid black line) and the data. The good fit to the data can be attributed to the fact that we have adjusted the ratio of the axisymmetric and asymmetric rotating components. For the hydrogen fit, the weights of the two contributions are approximately the same. This means the axisymmetric distribution produces about half the average signal. For the oxygen fit, the intensity of the axisymmetric distribution is about twice the intensity of the rotating piece. This implies that for some rotation phases, the symmetric component dominates the ENA signal. This is consistent with the persistence in the resolved oxygen images of the night side as the brightest region, even at times when the summed counts are at their minimum. For these plots, we have assumed the intensity of the parent ion population can be written as $j \sim E^{-\gamma}$ and that the ion spectrum for both species has an exponential falloff of $\gamma = 2.8$ (this value is derived from fits to the measured ENA spectra of both the H and the O).

[16] Finally it is important to mention that the Compton-Getting effect explains more than the brightening of images near midnight. It also explains the larger peak-to-valley ratio in the data in Figure 3 for oxygen. For the energies presented, the particle velocity is much closer to the convection speed for oxygen ENAs (4–6 keV/nucleon) than hydrogen ENAs (20–50 keV) and so the CG effect is larger for those particles.

4. Discussion

[17] In this paper, we have attempted to explain several features of INCA ENA images, focusing on a period late in 2004. Data suggest that a rotating feature often dominates the ENA signal from the inner magnetosphere. During approach to the planet, we observed periods dominated by a rotating population interspersed with quieter periods, accounting for the variation in the signal. We suggest here that some basic effects must be taken into account to begin to understand various features of these ENA images. These are the R^{-2} effect and the Compton-Getting effect; the latter has been overlooked in ENA imaging at Earth, where ring current convection speeds are much smaller. The relative importance of each of these two effects depends on the distance between the spacecraft and the rotating source, because the CG effect is independent of distance. The CG effect contributes to the brightening near midnight and the higher peak-to-valley ratios in the summed oxygen counts.

[18] We suggest, however, that the dynamics of this situation is complex so we believe that more work needs to be done to understand the source and loss processes more fully. The ENA signal by definition represents a loss process for ions and these data show the loss process has symmetric and asymmetric spatial features. Any longitudinally-symmetric processes, such as slow, inward radial diffusion, would power the symmetric component. Ion injections have been observed by *Mauk et al.* [2005], but more work needs to be done in understanding how deeply particles are injected, where peak losses are to the neutral cloud, how long an injected population survives, and whether and how it can be replenished. *Krupp et al.* (2005) prefer a picture in which the asymmetric part of the emission is associated with a specific longitude on the planet that becomes more intense following an injection. In any case, there will always be an R^{-2} dependence of ENA intensity from an unresolved source, while the Compton-Getting effect will modify the apparent brightness of ENA emission from an ion source moving with respect to the observing spacecraft.

References

Forman, M. (1970), The Compton-Getting effect for cosmic-ray particles and photons and the Lorentz invariance of distribution functions, *Planet. Space Sci.*, *18*, 25–31.

Gleeson, L. J., and W. I. Axford (1968), The Compton-Getting effect, *Astrophys. Space Sci.*, *2*, 431–437.

Ipavich, F. M. (1974), The Compton-Getting effect for low energy particles, *Geophys. Res. Lett.*, *1*, 149–152.

Krimigis, S. M., et al. (2005), Dynamics of Saturn's magnetosphere from MIMI during Cassini's orbital insertion, *Science*, *307*, 1270–1273.

Krimigis, S. M., et al. (2004), Magnetosphere imaging instrument (MIMI) on the Cassini mission to Saturn/Titan, *Space Sci. Rev.*, *114*, 233–329.

Krupp, N., et al. (2005), The Saturnian plasma sheet as revealed by energetic particle measurements, *Geophys. Res. Lett.*, *32*, L20S03, doi:10.1029/2005GL022829.

Mauk, B. H., et al. (2005), Energetic particle injections in Saturn's magnetosphere, *Geophys. Res. Lett.*, *32*, L14S05, doi:10.1029/2005GL022485.

Mitchell, D. G., C. P. Paranicas, B. H. Mauk, E. C. Roelof, and S. M. Krimigis (2004), Energetic neutral atoms from Jupiter measured with the Cassini magnetospheric imaging instrument: Time dependence and composition, *J. Geophys. Res.*, *109*, A09S11, doi:10.1029/2003JA010120.

Mitchell, D. G., et al. (1998), The imaging neutral camera for the Cassini mission to Saturn and Titan, in *Measurement Techniques in Space Plasmas: Fields*, *Geophys. Monogr. Ser.*, vol. 103, edited by R. F. Pfaff, J. E. Borovsky, and D. T. Young, pp. 281–287, AGU, Washington, D. C.

Paranicas, C., P. Brandt, D. Williams, D. Mitchell, E. Roelof, B. Mauk, and S. Krimigis (2005), The Compton-Getting effect in energetic neutral atom images of Saturn's magnetosphere, *Geophys. Res. Abstr.*, *7*, EGU05-A-02469.

Richardson, J. D. (1998), OH in Saturn's magnetosphere: Observations and implications, *J. Geophys. Res.*, *103*, 20,245–20,255.

Roelof, E. C., E. P. Keath, C. O. Bostron, and D. J. Williams (1976), Fluxes of >50 keV protons and >30 keV electrons at 35 R_E: 1. Velocity anisotropy and plasma from in the magnetotail, *J. Geophys. Res.*, *81*, 2304–2326.

Shemansky, D. E., L. Esposito, and Cassini UVIS Team (2004), Implications of Cassini UVIS observations of neutral gas in Saturn's magnetosphere, *Eos Trans. AGU*, *85*(47), Fall Meet. Suppl., Abstract P54A-01.

P. C. Brandt, S. M. Krimigis, B. H. Mauk, D. G. Mitchell, C. Paranicas, E. C. Roelof, and D. J. Williams, Applied Physics Laboratory, Johns Hopkins University, 11100 Johns Hopkins Road, Laurel, MD 20723, USA. (chris.paranicas@jhuapl.edu)